Geophysical Research Letters®

Key Points:

- Previous work shows that sea-surface temperature (SST) anomalies in the western North Pacific precede extratropical circulation anomalies
- Here we explore the relative roles of oceanic and atmospheric-forced SST anomalies in driving the lagged atmospheric response
- Only oceanic-forced SST anomalies in the western North Pacific are associated with robust circulation anomalies that lag the SST field

Observed Linkages Between the Atmospheric Circulation and Oceanic-Forced Sea-Surface Temperature Variability in the Western North Pacific

Casey R. Patrizio[1] and David W. J. Thompson[1]

[1]Department of Atmospheric Sciences, Colorado State University, Ft. Collins, CO, USA

Abstract Previous research suggests the extratropical atmospheric circulation responds to that sea-surface temperature (SST) variability in the western North Pacific. However, the relative roles of oceanic and atmospheric processes in driving the SST anomalies that, in turn, seemingly influence the atmospheric circulation are unclear. Here, we exploit a simple stochastic climate model to subdivide the SST variability in the Kuroshio-Oyashio Extension region into components forced by oceanic and atmospheric processes. We then probe the lead/lag relationships between the atmospheric circulation and both components of the SST variability. Importantly, only the oceanic-forced SST variability is associated with robust atmospheric anomalies that lag the SSTs by 1 month. The results are consistent with the surface heat fluxes associated with atmospheric and oceanic-forced components of the SST variability. Overall, the findings suggest that ocean dynamical processes in the western North Pacific play an important role in influencing the variability of the extratropical circulation.

Plain Language Summary The study explores the role of midlatitude ocean dynamics in climate variability over the North Pacific sector. Previous studies suggest that the atmospheric circulation responds to sea-surface temperature (SST) anomalies in midlatitude regions with strong oceanic currents, such as in the Kuroshio-Oyashio Extension (KOE) region of the North Pacific. However, the role of heat transport by the ocean circulations in driving such SST anomalies and, in turn, the atmospheric response remains unclear. To address this outstanding issue, we use a simple model of midlatitude SST variability to isolate the oceanic and atmospheric-driven components of SST variability in the KOE region. As in previous studies, an atmospheric circulation pattern is found to arise 1 month after SST anomalies in the KOE region during the winter season. Here it is shown that this pattern is strongly linked to the oceanic-driven component of the SST anomalies, but not the atmospheric-driven component. The findings thus provide novel evidence of the importance of midlatitude ocean dynamical processes for climate variability.

1. Introduction

There is increasing evidence that the atmosphere responds to midlatitude sea-surface temperature (SST) variability in the vicinity of strong oceanic currents, such as the Kuroshio-Oyashio Extension (KOE) region of the North Pacific (e.g., Frankignoul et al., 2011; Kwon et al., 2010; O'Reilly & Czaja, 2015; Révelard et al., 2016; Smirnov et al., 2015; Wills & Thompson, 2018; Yook et al., 2022). However, it remains unclear whether the atmospheric response arises from SST variability driven by oceanic or atmospheric dynamical processes. The distinction is important for at least two reasons: (a) SST anomalies driven by atmospheric and oceanic processes generally have different timescales and spatial-scales (e.g., Bishop et al., 2017; Small, Bryan, Bishop, Larson, et al., 2019; Zhang, 2017), and (b) the surface heat fluxes associated with atmospheric and oceanic-driven SST anomalies likewise have different timescales, spatial-scales, and amplitudes (e.g., Bishop et al., 2017; O'Reilly et al., 2016; Small, Bryan, Bishop, & Tomas, 2019). The distinct characteristics of atmospheric and oceanic-forced SST anomalies may thus lead to distinct atmospheric responses. In this study, we use a novel method to investigate the relative roles of oceanic and atmospheric-forced SST anomalies in the atmospheric response to KOE SST anomalies.

The atmospheric response to midlatitude SST anomalies is both complex and subtle in theory, which makes its detection challenging in practice. Linear quasigeostrophic theory predicts that the surface heat flux anomalies associated with midlatitude SST anomalies are balanced by horizontal temperature advection by the lower-tropospheric flow (Hoskins & Karoly, 1981). For example, the heat fluxes associated with warm SST anomalies are

balanced by cold advection from a low-level cyclonic anomaly east of the SST anomalies. However, the predicted circulation anomalies are weak and hence can be easily obscured by the strong internal variability of the extratropical atmosphere. The response is further complicated by nonlinear feedbacks between the atmospheric mean flow and transient eddies (e.g., Kushnir et al., 2002; Peng & Whitaker, 1999; Peng et al., 1997). In fact, the response often resembles the pattern of atmospheric variability that forces the SST anomalies in the first place (e.g., Peng & Robinson, 2001). For example, the nonlinear response to warm midlatitude SST anomalies is typically associated with warm advection from a low-level anticyclonic anomaly downstream of the SST anomalies (e.g., Deser et al., 2004, 2007; Ferreira & Frankignoul, 2005; Liu & Wu, 2004).

Nonetheless, with advances in observations and modeling systems over the last few decades, there is now considerable evidence that the atmospheric circulation responds to midlatitude SST anomalies, particularly in the vicinity of western boundary currents such as the KOE region (e.g., Frankignoul et al., 2011; Kwon & Deser, 2007; Kwon et al., 2010, 2011; O'Reilly & Czaja, 2015; Révelard et al., 2016, 2018; Smirnov et al., 2015; Taguchi et al., 2012; Wills & Thompson, 2018; Xu et al., 2011; Yook et al., 2022). For example, Wills and Thompson (2018) showed that observed SST anomalies in the KOE region are followed by an atmospheric pattern that broadly resembles the linear response to midlatitude SST anomalies described by Hoskins and Karoly (1981). A companion study to this paper (Yook et al., 2022) indicates that a similar atmospheric pattern emerges in atmospheric general circulation model experiments forced by SST anomalies in the KOE region. Various atmospheric responses have also been linked to other metrics of Kuroshio current variability (e.g., Frankignoul et al., 2011; O'Reilly & Czaja, 2015; Révelard et al., 2016; Smirnov et al., 2015), such as its meridional displacements (e.g., Frankignoul et al., 2011; Nakamura et al., 2012; Smirnov et al., 2015).

Here we are interested in understanding the relative importance of oceanic and atmospheric-driven SST anomalies in the inferred atmospheric response to KOE SST variability. To do so, we exploit a simple stochastic climate model that isolates the oceanic and atmospheric components of the observed SST variability. The key result is that a large-scale atmospheric circulation response to SST variability in the KOE region resembling that found in some previous studies (Frankignoul et al., 2011; Kwon et al., 2011; Wills & Thompson, 2018; Yook et al., 2022) arises from the oceanic-forced component of the SST variability, but *not* the atmospheric-forced component. The findings provide novel evidence of the importance of midlatitude ocean dynamical processes for extratropical climate variability.

2. Data and Methods

2.1. Observationally-Based Data Sources

The main data sources are objectively-analyzed surface turbulent heat fluxes and SSTs from OAFlux (Yu et al., 2008), and surface radiative heat fluxes, and sea-level pressure (SLP) from the ERA5 reanalysis (Hersbach et al., 2020). In all cases, monthly-mean data is used at 1° resolution over the 1980–2017 period. Monthly anomalies are computed by removing the linear trend and seasonal cycle from the fields. To minimize the remote effects of ENSO on the midlatitude variability, we remove the components of the fields that are linearly related to ENSO variability as estimated from the Niño 3.4 index. We do not lag the Niño 3.4 index relative to the data since the lag has no bearing on our conclusions (not shown).

Monthly anomalies in the ocean mixed-layer heat flux convergence, Q'_o, are calculated as a residual in the mixed-layer energy budget as follows:

$$Q'_o = C_o \frac{\partial T'}{\partial t} - Q'_s \tag{1}$$

Here, T' is the monthly SST anomaly, Q'_s is the monthly surface heat flux anomaly, and C_o is the mixed-layer heat capacity ($C_o = \rho c_p \overline{h}$, where $\overline{h}$ is a monthly-mean mixed-layer depth). Monthly-mean mixed-layer depths are used from the ocean state estimate, ECCO (Forget et al., 2015; Fukumori et al., 2017), which provides output from an ocean GCM (MITgcm) that has been constrained by ocean observations between 1992 and 2015. The pattern and magnitude of the mean mixed-layer depths from ECCO agrees reasonably well with other ocean reanalyzes and observational estimates (e.g., Carton & Giese, 2008; de Boyer Montégut et al., 2004; Forget et al., 2015; Holte et al., 2017).

2.2. The Simple Stochastic Climate Model

We use a simple stochastic climate model (Frankignoul & Hasselmann, 1977; Hasselmann, 1976) to isolate the oceanic and atmospheric-forced components of the observed SST variability. The model is described in detail in Patrizio and Thompson (2022), and only the most salient aspects are highlighted here.

In one of the simplest formulations of the stochastic climate model (e.g., Frankignoul & Hasselmann, 1977), SST anomalies (T') are forced by stochastic atmospheric variability via the surface heat fluxes (F_a) and damped via the surface heat flux feedback ($-\lambda_s T'$). That is:

$$C_o \frac{\partial T'}{\partial t} = F_a - \lambda_s T' \tag{2}$$

In the model used here, forcing and damping by ocean processes are included. The explicit representation of ocean processes in the model is motivated by widespread evidence that ocean dynamical processes play an important role in midlatitude SST variability, for example, in western boundary current regions (e.g., Bishop et al., 2017; Patrizio & Thompson, 2021, 2022; Roberts et al., 2017; Small, Bryan, Bishop, Larson, et al., 2019). In this case:

$$C_o \frac{\partial T'}{\partial t} = F_a + F_o - \lambda T' \tag{3}$$

where

$$\lambda = \lambda_s + \lambda_o \tag{4}$$

Here, F_o and $-\lambda_o T'$ are the oceanic forcing and damping terms, respectively, and $\lambda T'$ is the total damping by both the surface heat fluxes and ocean processes.

The ocean forcing term F_o accounts for ocean processes that force SST variability in the mixed layer, such as ocean eddy heat transport. Such an ocean forcing term has been included in simple models of midlatitude SST variability as a representation of "ocean weather" (e.g., Bishop et al., 2017; Cane et al., 2017; Smirnov et al., 2014; R. Wu et al., 2006) and advection by the wind-driven gyres (e.g., Czaja & Marshall, 2000; Marshall et al., 2001; Qiu et al., 2007). Ocean processes that act to damp temperature anomalies, such as vertical mixing, have also been discussed in studies that have used simple stochastic climate models to understand midlatitude climate variability (e.g., Alexander & Penland, 1996; Frankignoul, 1985; Frankignoul & Reynolds, 1983; Frankignoul et al., 1998; Hall & Manabe, 1997; Patrizio & Thompson, 2022). However, to our knowledge, such a model has not been used to understand the observed relationships between midlatitude oceanic-forced SSTs and atmospheric circulation anomalies.

In order to estimate the forcing and damping terms from observations, we follow the methods of Frankignoul and Kestenare (2002). In particular, the surface heat flux anomalies and ocean heat flux convergence anomalies (Q'_s and Q'_o) are linearly decomposed into a forcing term (Q^*_s and Q^*_o), and a feedback term ($\lambda_s T'$ and $\lambda_o T'$) as follows:

$$Q'_s = Q^*_s - \lambda_s T' \tag{5}$$

$$Q'_o = Q^*_o - \lambda_o T' \tag{6}$$

The damping coefficients (λ_s and λ_o) are estimated using the following expressions:

$$\lambda_s = -\frac{\overline{Q'_s T'_{-1}}}{\overline{T' T'_{-1}}} \tag{7}$$

$$\lambda_o = -\frac{\overline{Q'_o T'_{-1}}}{\overline{T' T'_{-1}}} \tag{8}$$

where T'_{-1} denotes the SST anomalies leading the surface heat fluxes or ocean heat convergence anomalies by 1 month. Thus the damping coefficient is defined as the component of the surface heat flux anomalies or ocean heat flux convergence anomalies that is linearly related to T' at a lag of 1 month (i.e., Q'_s or Q'_o lags T'), and the

forcing term is defined as the residual. In the formulation of the simple model (Equation 3), we set $F_a = Q_s^*$ and $F_o = Q_o^*$. Details of the analysis, including justification for the similar treatment of the surface heat flux and ocean heat flux convergence anomalies are provided in Patrizio and Thompson (2022).

2.3. Oceanic and Atmospheric-Forced SST Indices

To estimate the oceanic-forced component of the observed SST anomalies, the simple model outlined in the previous section is evaluated with the observed estimate of oceanic forcing ($F_o = Q_o^*$), but *without* the observed estimate of the atmospheric forcing ($F_a = 0$). In particular, we define T_{ocn} as the oceanic-forced component of the SST anomalies, which is computed as follows:

$$C_o \frac{\partial T_{ocn}}{\partial t} = F_o - \lambda T_{ocn} \qquad (9)$$

Likewise, we define T_{atm} as the atmospheric-forced component of the SST anomalies, which is computed as:

$$C_o \frac{\partial T_{atm}}{\partial t} = F_a - \lambda T_{atm} \qquad (10)$$

Equations 9 and 10 are then discretized at monthly resolution and integrated using a 1st order Runge-Kutta method (i.e., forward-difference) to obtain the time evolution of T_{ocn} and T_{atm}. Initial conditions are provided by the observed SSTs at the beginning of the observed record.

Figure 1a shows the log-ratio of the resulting variances in T_{ocn} to T_{atm} evaluated at each point in the North Pacific. Note that T_{ocn} and T_{atm} are evaluated using all months of the year, but Figure 1a highlights variances for the winter months (DJF). Results are similar for other seasons. The variance of T_{ocn} exceeds the variance of T_{atm} in the KOE current region and its associated extension, but the opposite is generally true in the eastern basin where atmospheric forcing of SSTs is large (e.g., Smirnov et al., 2014). Since some previous studies have interpreted Ekman transport as an atmospheric forcing, we also tested how the ratio of oceanic to atmospheric forced SST variances changes when the horizontal Ekman transport—as computed from surface wind-stresses from ERA5— is excluded from the calculation of T_{ocn} and included in T_{atm}. When using these modified definitions of the SST indices, the ratio of variances in T_{ocn} to T_{atm} are reduced, especially in the eastern part of the basin (see Figure S1a in Supporting Information S1). However the variances of T_{ocn} still generally exceeds those of T_{atm} along the Kuroshio current region.

Throughout the rest of the study, we focus on SSTs averaged over the KOE region (37–44°N, 140–171°E) indicated by the black box in Figure 1a. This region has been the focus of many previous studies because it is a region with marked ocean dynamical activity, as supported by Figure 1a. The observed SSTs (T) and the components linked to oceanic and atmospheric processes (T_{ocn} and T_{atm}) are averaged over the KOE region to provide area-averaged indices of the oceanic- and atmospheric-forced SST anomalies in the KOE region. Monthly SLP anomalies are then linearly regressed onto the area-averaged SST indices to understand the relationships between the atmospheric circulation and the different components of the observed SST variability in the KOE region. We focus primarily on winter months (DJF) when air-sea interactions are generally the most intense, and thus when oceanic variability may have the strongest impact on the atmosphere.

3. Results

Figures 1b–1d show the KOE-averaged observed SST anomalies (T; gray) superposed on the associated estimates of oceanic-forced SST anomalies (T_{ocn}; purple in Figure 1b) and atmospheric-forced SST anomalies (T_{atm}; orange in Figure 1c). The sum of the atmospheric and oceanic components (black in Figure 1d) agrees well with observed SST index (gray), which is expected since the ocean heat flux convergence anomalies have been estimated indirectly as a residual in the mixed-layer energy budget.

The observational uncertainty in the SST indices is small, as quantified by observational uncertainty in the SSTs and air-sea heat fluxes provided by the OAFlux product. The mean-squared observational uncertainty is ± 0.002 K^2 for the T index, ± 0.02 K^2 for the T_{ocn} index, and ± 0.006 K^2 for the T_{atm} index. Other sources of
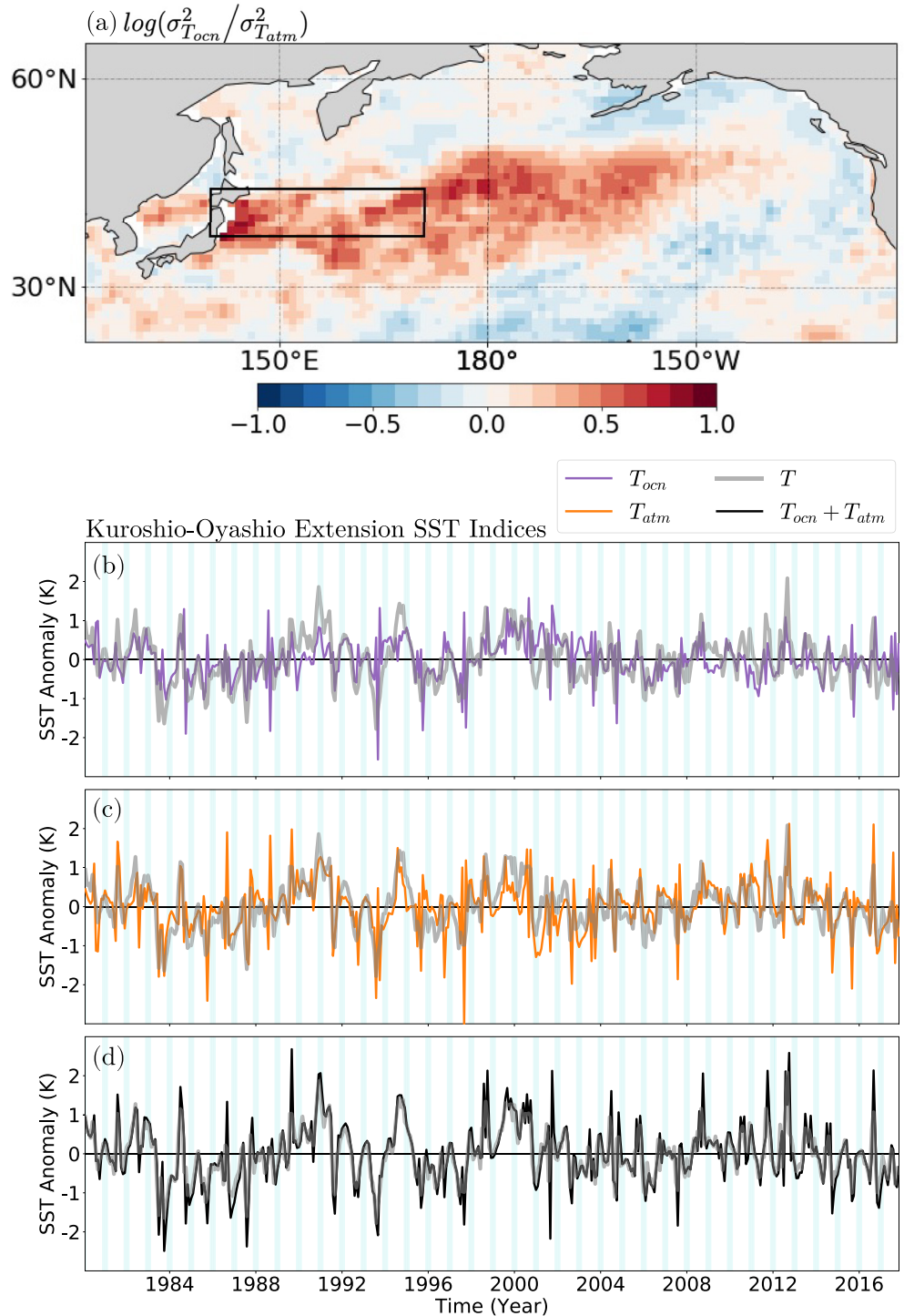
Figure 1. (a) Log-ratios of the wintertime (DJF) variances of ocean-forced sea-surface temperature (SSTs; T_{ocn}) to atmospheric-forced SSTs (T_{atm}) in the North Pacific basin. (b–d) The time evolution of atmospheric-forced (purple in b), atmospheric-forced (orange in c), and atmospheric plus oceanic forced (black in d) SST anomalies averaged over the Kuroshio-Oyashio Extension region, as in indicated by the black box in (a). Gray lines in (b–d) show the raw SST time series. Teal stripes indicate the winter (DJF) season.

observational uncertainty related to, for example, the monthly mean mixed-layer depths, are not accounted for here and could also contribute to uncertainty in our estimates of T_{atm} and T_{ocn}.

Figures 1b–1d indicate that both T_{ocn} and T_{atm} contribute to variability in the observed SSTs averaged over the KOE region. In contrast to the grid point results shown in Figure 1a, a large fraction of the variance of the SSTs averaged over the entire KOE region are due to atmospheric processes: that is, the variance of the T_{atm} index *exceeds* that of the T_{ocn} index, such that ∼40% of the KOE-averaged SST variance during winter is forced by the ocean. The distinctions between the variances of grid point and spatially-averaged SSTs suggests that a substantial fraction of oceanic-forced SST variance in the KOE region as shown in Figure 1a derives from small-scale eddy-driven heat transport which effectively cancels out when averaged over KOE region. It is also important to note that the T_{ocn} and T_{atm} indices are both strongly correlated with the full SST index ($r \sim 0.6$ and $r \sim 0.7$ during winter, respectively), but are not significantly correlated with each other.

The near-zero correlation between T_{ocn} and T_{atm} indicates that ocean and atmospheric-forced SST variability in the KOE region are not linearly related at zero lag. Previous studies have argued that a component of interannual to decadal SST variability in the KOE region reflects a lagged response of the ocean circulation to remote wind-stress forcing in the central and eastern North Pacific basin (e.g., Kwon & Deser, 2007; Kwon et al., 2010; Qiu et al., 2007; Wills et al., 2019). However, we find no statistically significant correlation between the SLP field in the North Pacific and the T_{ocn} index for lag times of up to 5 years (not shown). Thus the T_{ocn} index is not clearly linked to large-scale wind forcing at any lag. We defer a more comprehensive diagnosis of the processes that drive T_{ocn} to future work.

Figure 2 shows the SLP and SST anomalies regressed onto all three KOE SST indices (T, T_{ocn} and T_{atm}) as a function of lag. Note that the indices are standardized before performing the linear regression. Results at negative lags indicate the SLP and SST fields lead the KOE indices, and positive lags indicate vice versa. Figure 3 shows the associated significance of the SLP anomalies, as measured by a two-tailed test of Student's t-statistic.

The SLP and SST regression patterns associated with the full KOE SST index (Figures 2a–2c) generally support previous findings. By construction, the SST anomalies are dominated by warm SST anomalies that peak in the western North Pacific at lag 0. The SLP pattern that *leads* the SST index (Figure 2a) is dominated by high-pressure anomalies in the North Pacific. The anomalies are associated with warm advection over the KOE region and hence forcing of SST anomalies there (e.g., Deser & Timlin, 1997; Kushnir et al., 2002). They may be viewed as the "atmospheric forcing" of the SST field (e.g., Wills & Thompson, 2018).

The SLP pattern that *lags* the full KOE index SST index by 1 month is dominated by low-pressure anomalies in the North Pacific (Figure 2c). In this case, the SLP anomalies are consistent with the linear atmospheric response to midlatitude SST anomalies, in which heating due to the SST anomaly is balanced by cold advection by the atmospheric flow (Hoskins & Karoly, 1981). As the atmospheric circulation anomalies are distinct from the "atmospheric forcing" pattern, they may be viewed as the "atmospheric response" to the SST anomalies at lag 0 (e.g., Wills & Thompson, 2018). Note that, in this study, we focus on the atmospheric circulation anomalies at a lag of 1 month because we do not find any distinct circulation anomalies at later times (see Figure S2 in Supporting Information S1). The North Pacific SLP anomalies found at positive lag are broadly consistent with the atmospheric response to KOE SST anomalies inferred in several previous studies (e.g., Frankignoul et al., 2011; Kwon et al., 2011; Wills & Thompson, 2018; Yook et al., 2022). However, the literature is not conclusive on the atmospheric response to KOE SST variability, and the results shown here also contradict the sign of the response inferred in several other studies (e.g., Révelard et al., 2016; Taguchi et al., 2012). The reasons for the discrepancies in the inferred atmospheric response between previous studies is unclear.

The SLP regression maps at both positive and negative lags are also marked by anomalies outside the North Pacific sector. It is likely that the remote anomalies at negative lags arise from teleconnectivity inherent in the SLP field associated with the atmospheric forcing anomalies. For example, the annular mode is weakly apparent in Figure 2a. On the other hand, the cause of the remote SLP anomalies at positive lags is not clear. Such anomalies could arise in the absence of ocean forcing due to the persistence of the atmospheric forcing anomalies, but could also reflect a remote response to heating anomalies in the North Pacific sector. The remote circulation anomalies are not recovered in the simulated response to KOE SST anomalies found in the companion paper (Yook et al., 2022), and are thus less robust than the SLP anomalies centered over the North Pacific.
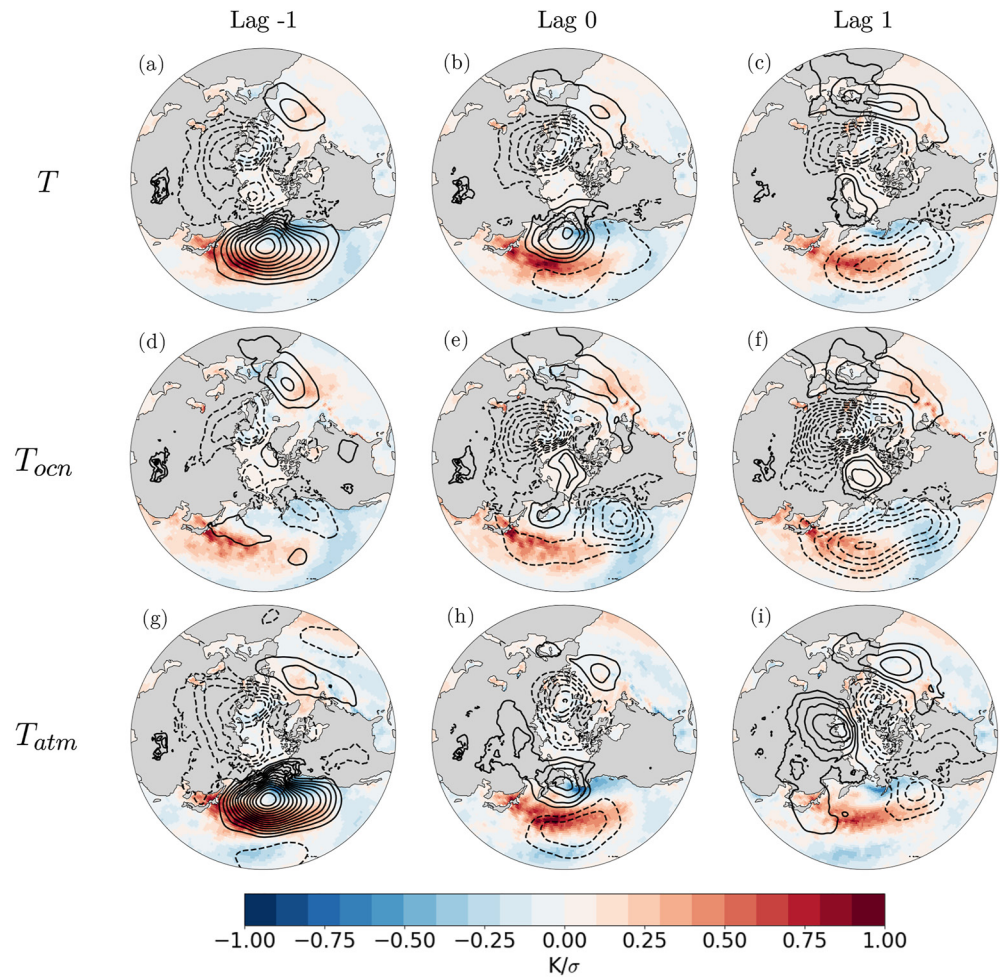
Figure 2. (Top row) Wintertime sea level pressure (SLP) (contours) and sea-surface temperature (SST) (shading) anomalies regressed onto standardized values of the Kuroshio-Oyashio Extension SST index at lags ranging from −1 month to +1 month. Negative lag denotes the SLP and SST fields leading the SST index by 1 month, and positive lag indicates vice versa. (Middle and bottom rows) As in the top row, except for regressions based on standardized values of the oceanic-forced SST index (middle row) and atmospheric-forced SST index (bottom row). The contour interval is 0.4 hPa; dashed lines denote negative values.

The results shown in the middle and bottom rows of Figure 2 show analogous results, but for regressions based on the oceanic (T_{ocn}) and atmospheric (T_{atm}) components of the KOE SST index. To first order, the SST patterns associated with the T, T_{ocn} and T_{atm} indices bear strong resemblance to each other. However, there are some differences. Notably, the SST pattern associated with T_{ocn} (Figures 2d–2f) generally has largest amplitudes in a narrow region in the vicinity of the KOE region, consistent with local oceanic forcing, whereas the SST pattern associated with T_{atm} (Figures 2g–2i) has largest amplitudes over a much broader region, consistent with relatively large-scale atmospheric forcing.

In contrast, the SLP patterns associated with T_{ocn} and T_{atm} exhibit very different structures from each other. Comparing the top and middle rows in Figure 2, it is clear that the high-pressure anomalies that lead the SST variability in the regressions based on the full SST index (T) are only apparent in regressions based on the component of the SSTs forced by atmospheric processes (T_{atm}). The results thus support the interpretation that the pattern of high-pressure anomalies at negative lag reflects the forcing of the SST field by atmospheric processes. Since T_{ocn} is not associated with a distinct pattern of atmospheric circulation anomalies at negative lag, the results also support the interpretation that pattern of SST anomalies associated with T_{ocn} is driven by ocean dynamical processes.
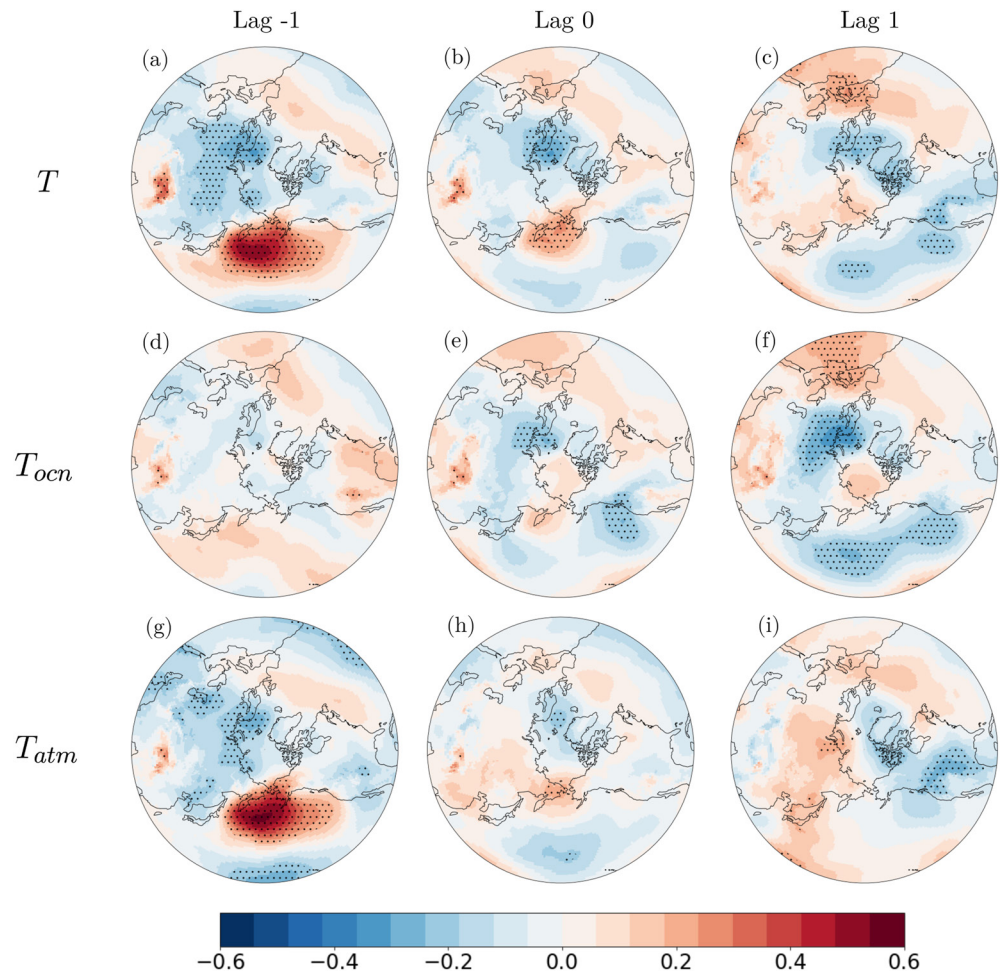
Figure 3. As in Figure 2, except for the correlation between sea level pressure anomalies and the full (top), oceanic-forced (middle), and atmospheric-forced (bottom) Kuroshio-Oyashio Extension sea-surface temperature indices. Stippling indicates grid points that are statistically significant at the 95% level as measured by a two-tailed test of Student's t-statistic.

Importantly, the low-pressure anomalies in the North Pacific that lag the observed SST index by 1 month (Figure 2c) are only apparent in regressions based on the component of the SSTs forced by ocean processes. In fact, the SLP anomalies that lag T_{ocn} are even more pronounced than those that lag the full SST index (compare Figures 2c and 2f). Hence, only oceanic-forced SST variability in the KOE region is linked to the basin-wide low-pressure anomalies at a lag of 1 month. The regressions based on the T_{ocn} index also account for the vast majority of the SLP anomalies that extend beyond the North Pacific sector. We also note that the atmospheric circulation anomalies lagging T_{ocn} are very similar when the horizontal Ekman transport is included in our calculation of T_{atm} rather than T_{ocn}, which suggests that the apparent atmospheric response derives from non-Ekman heat transport (see Figure S1c in Supporting Information S1).

4. Interpretation

The results in Figure 2 reveal that (a) the pattern of high-pressure anomalies that *precedes* KOE SST variability by 1 month derives from the component of the KOE SST variability linked to atmospheric processes whereas (b) the pattern of low-pressure anomalies that *lags* KOE SST variability by 1 month derives from the component linked to oceanic processes. This key result is highly significant. It is significant at the 95% confidence level based on the t-statistic (Figure 3) and is reproducible in analyses repeated for the first and second halves of the data record (not shown).
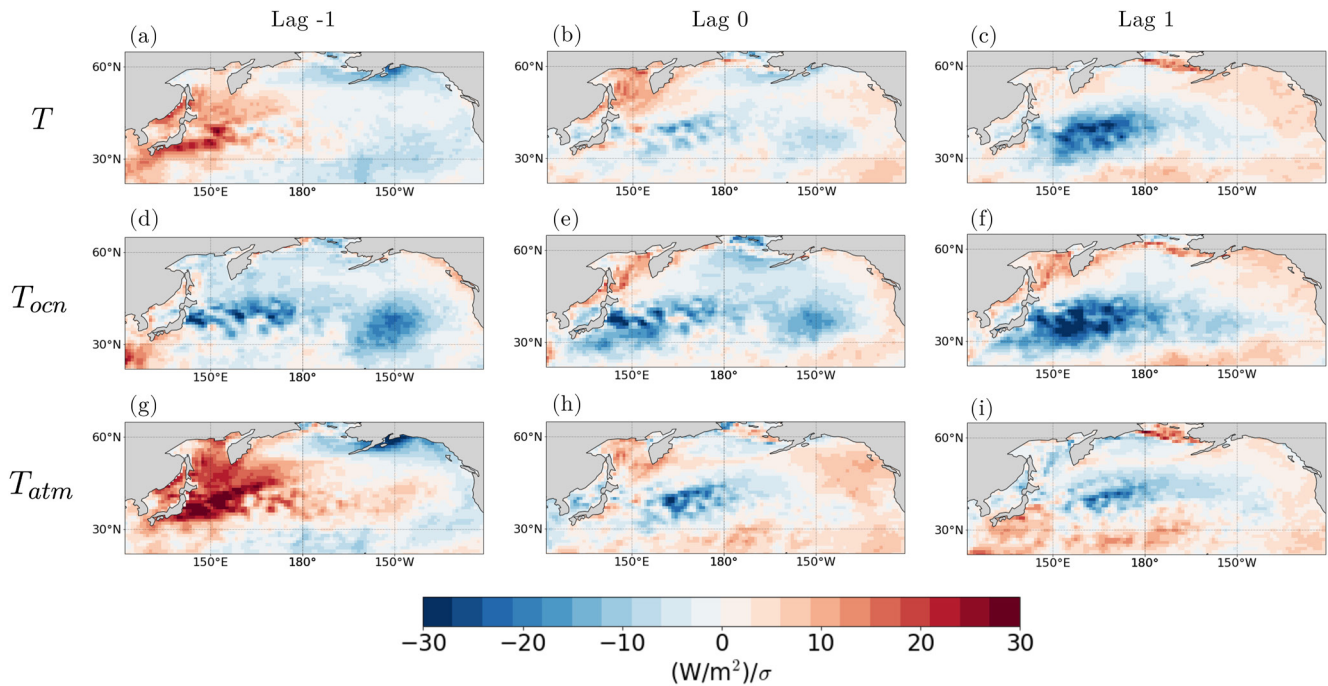
Figure 4. As in Figure 2, except for surface heat flux anomalies (W/m²) regressed onto the full (top), oceanic-forced (middle), and atmospheric-forced (bottom) Kuroshio-Oyashio Extension sea-surface temperature indices. Cool colors indicate heat loss from the surface to the atmosphere and warm colors indicate heat gain by the surface.

In principle, the atmosphere does not care whether the underlying SST anomalies are driven by atmospheric or oceanic processes. So at first glance it is unclear why the inferred atmospheric response at a lag of 1 month is only apparent in association with the ocean-forced component of the SST field. The result is particularly intriguing because the variance of the T_{atm} index exceeds the variance of the T_{ocn} index and both indices are associated with similar SST patterns.

Insight into this apparent paradox can be gained from maps formed by regressing the surface heat flux anomalies onto the three KOE SST indices. As evidenced in Figure 4, the T_{ocn} index is associated with large heat losses by the ocean at all lags, whereas the T_{atm} index is associated with heat gains prior to the peak of the SST anomaly, and weak heat losses during and after the peak of the SST anomaly. When averaged over the KOE region and all lags, the surface heat flux anomaly associated with variability in T_{ocn} is -12.1 W/m² (heat lost by the ocean and *gained* by the atmosphere), whereas the surface heat flux anomaly with variability in T_{atm} is 1.4 W/m² (heat gained by the ocean and *lost* by the atmosphere).

The results shown in Figure 4 thus suggest that the oceanic-forced component of the KOE SST variability is marked by more persistent heat loss to the atmosphere than the atmospheric-forced component of the KOE SST variability. Indeed, the lag-autocorrelation of the T_{ocn} index exceeds that of the T_{atm} index: the 1-month lag-autocorrelation is ~0.40 for T_{ocn} and ~0.26 for T_{atm}. This is consistent with results from Patrizio and Thompson (2022), who showed that the power spectra of the observed estimate of the oceanic forcing is generally redder than that of the atmospheric forcing throughout the midlatitude oceans. It also supports existing evidence that ocean dynamical processes are generally redder than their atmospheric counterparts (e.g., Bjerknes, 1964; Gulev et al., 2013). The results shown in Figure 4 are also consistent with previous studies that have shown that atmospheric-driven SST variability is generally associated with opposite signed surface heat flux anomalies at positive and negative lag, whereas oceanic-driven SST variability is generally associated with heat loss to the atmosphere at both positive and negative lag (e.g., Bishop et al., 2017; O'Reilly et al., 2016). Here, our results suggest that the persistence—and thus low-frequency magnitude— of the surface heat flux anomalies associated with ocean-forced SST anomalies explains why they have a very different signature in the atmospheric circulation than atmospheric-forced SST anomalies.

5. Concluding Remarks

The key finding in this study is that the pattern of atmospheric circulation anomalies that lags SST anomalies in the KOE region by about 1 month arises only from the component of the SST variability that is driven by ocean dynamical processes. In the case of positive SST anomalies, the results suggest that the atmospheric response includes significant low-level cyclonic anomalies that span the North Pacific when the SST anomalies are driven by ocean dynamics. The cyclonic anomalies are broadly consistent with the theoretical linear response to thermal forcing (Hoskins & Karoly, 1981), as well as the simulated response to KOE anomalies found in the companion paper (Yook et al., 2022).

We have speculated that the differences in the atmospheric responses to ocean-forced and atmospheric-forced KOE SST anomalies arise from the timescales of the attendant surface heat fluxes. In the case of warm SST anomalies, the atmospheric-forced component is associated with heat fluxes out of the ocean at positive lag but into the ocean at negative lag. In contrast, the ocean-forced component is associated with fluxes out of the ocean at all lags. Thus the heat fluxes out of the ocean associated with ocean-forced SST anomalies are more persistent—and thus have larger amplitude averaged over all lags—than those associated with atmospheric-forced SST anomalies. This result is particularly intriguing because our decomposition methodology also suggests that the atmospheric-forced SST anomalies are larger than oceanic-forced SST anomalies when averaged over the KOE region. The results therefore emphasize the importance of considering surface heat flux anomalies rather than SST anomalies when exploring the atmospheric response to variations in the midlatitude SST field, as has been argued by several previous studies (e.g., O'Reilly et al., 2016; Sutton & Mathieu, 2002; P. Wu & Rodwell, 2003; Yulaeva et al., 2001).

Together, the results shown here contribute to a growing body of evidence that indicates ocean dynamical processes in the western North Pacific play an important role in extratropical climate variability. The physical consistency of results based on our decomposition methodology suggest that the methodology could be readily extended to explore the role of ocean dynamics in driving climate variability over other ocean basins.

Data Availability Statement

The observational and reanalysis data used in this study are available at the following links as netCDF files. Sea-surface temperatures, latent heat fluxes and sensible heat fluxes from OAFlux can be downloaded from the Research Data Archive (RDA) at the following link (select the data files with prefixes "ts", "lh", and "sh", respectively): https://rda.ucar.edu/datasets/ds260.1/index.html#sfol-wl-/data/ds260.1?g=2. To access the OAFlux data, a UCAR RDA account must first be created here: https://rda.ucar.edu/index.html?hash=data_user&action=register. Mixed-layer depths from ECCO can be downloaded at the following link: https://ecco.jpl.nasa.gov/drive/files/Version4/Release3/interp_monthly/MXLDEPTH. To access the ECCO data, a NASA EarthData account must first be created here: https://urs.earthdata.nasa.gov/home. Net surface radiation and sea level pressure from ERA5 reanalysis can be downloaded from the Climate Data Store at the following link (select "surface net solar radiation", "surface net thermal radiation", and "mean SLP"): https://cds.climate.copernicus.eu/cdsapp#!/dataset/reanalysis-era5-single-levels-monthly-means?tab=form.

References

Alexander, M. A., & Penland, C. (1996). Variability in a mixed layer ocean model driven by stochastic atmospheric forcing. *Journal of Climate*, *9*(10), 2424–2442. https://doi.org/10.1175/1520-0442(1996)009<2424:viamlo>2.0.co;2

Bishop, S. P., Small, R. J., Bryan, F. O., & Tomas, R. A. (2017). Scale dependence of midlatitude air–sea interaction. *Journal of Climate*, *30*(20), 8207–8221. https://doi.org/10.1175/jcli-d-17-0159.1

Bjerknes, J. (1964). Atlantic air-sea interaction. In *Advances in Geophysics*, (Vol. 10, pp. 1–82). Elsevier. https://doi.org/10.1016/s0065-2687(08)60005-9

Cane, M. A., Clement, A. C., Murphy, L. N., & Bellomo, K. (2017). Low-pass filtering, heat flux, and Atlantic multidecadal variability. *Journal of Climate*, *30*(18), 7529–7553. https://doi.org/10.1175/jcli-d-16-0810.1

Carton, J. A., & Giese, B. S. (2008). A reanalysis of ocean climate using Simple Ocean Data Assimilation (SODA). *Monthly Weather Review*, *136*(8), 2999–3017. https://doi.org/10.1175/2007mwr1978.1

Czaja, A., & Marshall, J. (2000). On the interpretation of AGCMs response to prescribed time-varying SST anomalies. *Geophysical Research Letters*, *27*(13), 1927–1930. https://doi.org/10.1029/1999gl011322

de Boyer Montégut, C., Madec, G., Fischer, A. S., Lazar, A., & Iudicone, D. (2004). Mixed layer depth over the global ocean: An examination of profile data and a profile-based climatology. *Journal of Geophysical Research*, *109*(C12), C12003. https://doi.org/10.1029/2004jc002378

Deser, C., Phillips, A. S., & Hurrell, J. W. (2004). Pacific interdecadal climate variability: Linkages between the tropics and the North Pacific during boreal winter since 1900. *Journal of Climate*, *17*(16), 3109–3124. https://doi.org/10.1175/1520-0442(2004)017<3109:picvlb>2.0.co;2

Deser, C., & Timlin, M. S. (1997). Atmosphere–ocean interaction on weekly timescales in the North Atlantic and Pacific. *Journal of Climate*, *10*(3), 393–408. https://doi.org/10.1175/1520-0442(1997)010<0393:aoiowt>2.0.co;2

Deser, C., Tomas, R. A., & Peng, S. (2007). The transient atmospheric circulation response to North Atlantic SST and sea ice anomalies. *Journal of Climate*, *20*(18), 4751–4767. https://doi.org/10.1175/jcli4278.1

Ferreira, D., & Frankignoul, C. (2005). The transient atmospheric response to midlatitude SST anomalies. *Journal of Climate*, *18*(7), 1049–1067. https://doi.org/10.1175/jcli-3313.1

Forget, G., Campin, J.-M., Heimbach, P., Hill, C. N., Ponte, R. M., & Wunsch, C. (2015). *ECCO version 4: An integrated framework for non-linear inverse modeling and global ocean state estimation*.

Frankignoul, C. (1985). Sea surface temperature anomalies, planetary waves, and air-sea feedback in the middle latitudes. *Reviews of Geophysics*, *23*(4), 357–390. https://doi.org/10.1029/rg023i004p00357

Frankignoul, C., Czaja, A., & L'Heveder, B. (1998). Air–sea feedback in the North Atlantic and surface boundary conditions for ocean models. *Journal of Climate*, *11*(9), 2310–2324. https://doi.org/10.1175/1520-0442(1998)011<2310:asfitn>2.0.co;2

Frankignoul, C., & Hasselmann, K. (1977). Stochastic climate models, Part II: Application to sea-surface temperature anomalies and thermocline variability. *Tellus*, *29*(4), 289–305. https://doi.org/10.3402/tellusa.v29i4.11362

Frankignoul, C., & Kestenare, E. (2002). The surface heat flux feedback. Part I: Estimates from observations in the Atlantic and the North Pacific. *Climate Dynamics*, *19*(8), 633–647.

Frankignoul, C., & Reynolds, R. W. (1983). Testing a dynamical model for mid-latitude sea surface temperature anomalies. *Journal of Physical Oceanography*, *13*(7), 1131–1145. https://doi.org/10.1175/1520-0485(1983)013<1131:tadmfm>2.0.co;2

Frankignoul, C., Sennéchael, N., Kwon, Y.-O., & Alexander, M. A. (2011). Influence of the meridional shifts of the Kuroshio and the Oyashio Extensions on the atmospheric circulation. *Journal of Climate*, *24*(3), 762–777. https://doi.org/10.1175/2010jcli3731.1

Fukumori, I., Wang, O., Fenty, I., Forget, G., Heimbach, P., & Ponte, R. M. (2017). *ECCO version 4 release 3 (Tech. Rep.)*.

Gulev, S. K., Latif, M., Keenlyside, N., Park, W., & Koltermann, K. P. (2013). North Atlantic Ocean control on surface heat flux on multidecadal timescales. *Nature*, *499*(7459), 464–467. https://doi.org/10.1038/nature12268

Hall, A., & Manabe, S. (1997). Can local linear stochastic theory explain sea surface temperature and salinity variability? *Climate Dynamics*, *13*(3), 167–180. https://doi.org/10.1007/s003820050158

Hasselmann, K. (1976). Stochastic climate models part I. Theory. *Tellus*, *28*(6), 473–485. https://doi.org/10.3402/tellusa.v28i6.11316

Hersbach, H., Bell, B., Berrisford, P., Hirahara, S., Horányi, A., Muñoz-Sabater, J., et al. (2020). The ERA5 global reanalysis. *Quarterly Journal of the Royal Meteorological Society*, *146*(730), 1999–2049. https://doi.org/10.1002/qj.3803

Holte, J., Talley, L. D., Gilson, J., & Roemmich, D. (2017). An Argo mixed layer climatology and database. *Geophysical Research Letters*, *44*(11), 5618–5626. https://doi.org/10.1002/2017gl073426

Hoskins, B. J., & Karoly, D. J. (1981). The steady linear response of a spherical atmosphere to thermal and orographic forcing. *Journal of the Atmospheric Sciences*, *38*(6), 1179–1196. https://doi.org/10.1175/1520-0469(1981)038<1179:tslroa>2.0.co;2

Kushnir, Y., Robinson, W., Bladé, I., Hall, N., Peng, S., & Sutton, R. (2002). Atmospheric GCM response to extratropical SST anomalies: Synthesis and evaluation. *Journal of Climate*, *15*(16), 2233–2256. https://doi.org/10.1175/1520-0442(2002)015<2233:agrtes>2.0.co;2

Kwon, Y.-O., Alexander, M. A., Bond, N. A., Frankignoul, C., Nakamura, H., Qiu, B., & Thompson, L. A. (2010). Role of the Gulf Stream and Kuroshio–Oyashio systems in large-scale atmosphere–ocean interaction: A review. *Journal of Climate*, *23*(12), 3249–3281. https://doi.org/10.1175/2010jcli3343.1

Kwon, Y.-O., & Deser, C. (2007). North Pacific decadal variability in the community climate system model version 2. *Journal of Climate*, *20*(11), 2416–2433. https://doi.org/10.1175/jcli4103.1

Kwon, Y.-O., Deser, C., & Cassou, C. (2011). Coupled atmosphere–mixed layer ocean response to ocean heat flux convergence along the Kuroshio Current Extension. *Climate Dynamics*, *36*(11–12), 2295–2312. https://doi.org/10.1007/s00382-010-0764-8

Liu, Z., & Wu, L. (2004). Atmospheric response to North Pacific SST: The role of ocean–atmosphere coupling. *Journal of Climate*, *17*(9), 1859–1882. https://doi.org/10.1175/1520-0442(2004)017<1859:artnps>2.0.co;2

Marshall, J., Johnson, H., & Goodman, J. (2001). A study of the interaction of the North Atlantic Oscillation with ocean circulation. *Journal of Climate*, *14*(7), 1399–1421. https://doi.org/10.1175/1520-0442(2001)014<1399:asotio>2.0.co;2

Nakamura, H., Nishina, A., & Minobe, S. (2012). Response of storm tracks to bimodal Kuroshio path states south of Japan. *Journal of Climate*, *25*(21), 7772–7779. https://doi.org/10.1175/jcli-d-12-00326.1

O'Reilly, C. H., & Czaja, A. (2015). The response of the Pacific storm track and atmospheric circulation to Kuroshio Extension variability. *Quarterly Journal of the Royal Meteorological Society*, *141*(686), 52–66.

O'Reilly, C. H., Huber, M., Woollings, T., & Zanna, L. (2016). The signature of low-frequency oceanic forcing in the Atlantic Multidecadal Oscillation. *Geophysical Research Letters*, *43*(6), 2810–2818.

Patrizio, C. R., & Thompson, D. W. (2021). Quantifying the role of ocean dynamics in ocean mixed-layer temperature variability. *Journal of Climate*, *34*(7), 2567–2589. https://doi.org/10.1175/jcli-d-20-0476.1

Patrizio, C. R., & Thompson, D. W. (2022). Understanding the role of ocean dynamics in midlatitude sea surface temperature variability using a simple stochastic climate model. *Journal of Climate*, 1–62. https://doi.org/10.1175/JCLI-D-21-0184.1

Peng, S., & Robinson, W. A. (2001). Relationships between atmospheric internal variability and the responses to an extratropical SST anomaly. *Journal of Climate*, *14*(13), 2943–2959. https://doi.org/10.1175/1520-0442(2001)014<2943:rbaiva>2.0.co;2

Peng, S., Robinson, W. A., & Hoerling, M. P. (1997). The modeled atmospheric response to midlatitude SST anomalies and its dependence on background circulation states. *Journal of Climate*, *10*(5), 971–987. https://doi.org/10.1175/1520-0442(1997)010<0971:tmartm>2.0.co;2

Peng, S., & Whitaker, J. S. (1999). Mechanisms determining the atmospheric response to midlatitude SST anomalies. *Journal of Climate*, *12*(5), 1393–1408. https://doi.org/10.1175/1520-0442(1999)012<1393:mdtart>2.0.co;2

Qiu, B., Schneider, N., & Chen, S. (2007). Coupled decadal variability in the North Pacific: An observationally constrained idealized model. *Journal of Climate*, *20*(14), 3602–3620. https://doi.org/10.1175/jcli4190.1

Révelard, A., Frankignoul, C., & Kwon, Y.-O. (2018). A multivariate estimate of the cold season atmospheric response to North Pacific SST variability. *Journal of Climate*, *31*(7), 2771–2796. https://doi.org/10.1175/jcli-d-17-0061.1

Révelard, A., Frankignoul, C., Sennéchael, N., Kwon, Y.-O., & Qiu, B. (2016). Influence of the decadal variability of the Kuroshio Extension on the atmospheric circulation in the cold season. *Journal of Climate*, *29*(6), 2123–2144. https://doi.org/10.1175/jcli-d-15-0511.1

Roberts, C. D., Palmer, M. D., Allan, R. P., Desbruyeres, D. G., Hyder, P., Liu, C., & Smith, D. (2017). Surface flux and ocean heat transport convergence contributions to seasonal and interannual variations of ocean heat content. *Journal of Geophysical Research: Oceans*, *122*(1), 726–744. https://doi.org/10.1002/2016jc012278

Small, R. J., Bryan, F. O., Bishop, S. P., Larson, S., & Tomas, R. A. (2019). What drives upper-ocean temperature variability in coupled climate models and observations? *Journal of Climate*, *33*(2), 577–596.

Small, R. J., Bryan, F. O., Bishop, S. P., & Tomas, R. A. (2019). Air–sea turbulent heat fluxes in climate models and observational analyses: What drives their variability? *Journal of Climate*, *32*(8), 2397–2421. https://doi.org/10.1175/jcli-d-18-0576.1

Smirnov, D., Newman, M., & Alexander, M. A. (2014). Investigating the role of ocean–atmosphere coupling in the North Pacific Ocean. *Journal of Climate*, *27*(2), 592–606. https://doi.org/10.1175/jcli-d-13-00123.1

Smirnov, D., Newman, M., Alexander, M. A., Kwon, Y.-O., & Frankignoul, C. (2015). Investigating the local atmospheric response to a realistic shift in the Oyashio sea surface temperature front. *Journal of Climate*, *28*(3), 1126–1147. https://doi.org/10.1175/jcli-d-14-00285.1

Sutton, R., & Mathieu, P.-P. (2002). Response of the atmosphere–ocean mixed-layer system to anomalous ocean heat-flux convergence. *Quarterly Journal of the Royal Meteorological Society: A journal of the atmospheric sciences, applied meteorology and physical oceanography*, *128*(582), 1259–1275. https://doi.org/10.1256/003590002320373283

Taguchi, B., Nakamura, H., Nonaka, M., Komori, N., Kuwano-Yoshida, A., Takaya, K., & Goto, A. (2012). Seasonal evolutions of atmospheric response to decadal SST anomalies in the North Pacific subarctic frontal zone: Observations and a coupled model simulation. *Journal of Climate*, *25*(1), 111–139. https://doi.org/10.1175/jcli-d-11-00046.1

Wills, R. C., Battisti, D. S., Proistosescu, C., Thompson, L., Hartmann, D. L., & Armour, K. C. (2019). Ocean circulation signatures of North Pacific decadal variability. *Geophysical Research Letters*, *46*(3), 1690–1701. https://doi.org/10.1029/2018gl080716

Wills, S. M., & Thompson, D. W. (2018). On the observed relationships between wintertime variability in Kuroshio–Oyashio extension sea surface temperatures and the atmospheric circulation over the North Pacific. *Journal of Climate*, *31*(12), 4669–4681. https://doi.org/10.1175/jcli-d-17-0343.1

Wu, P., & Rodwell, M. J. (2003). Gulf stream forcing of the winter North Atlantic oscillation. *Atmospheric Science Letters*, *5*(1–4), 57–64. https://doi.org/10.1016/j.atmoscilet.2003.12.002

Wu, R., Kirtman, B. P., & Pegion, K. (2006). Local air–sea relationship in observations and model simulations. *Journal of Climate*, *19*(19), 4914–4932. https://doi.org/10.1175/jcli3904.1

Xu, H., Xu, M., Xie, S.-P., & Wang, Y. (2011). Deep atmospheric response to the spring Kuroshio over the East China Sea. *Journal of Climate*, *24*(18), 4959–4972. https://doi.org/10.1175/jcli-d-10-05034.1

Yook, S., Thompson, D. W., Sun, L., & Patrizio, C. R. (2022). The simulated atmospheric response to western North Pacific sea-surface temperature anomalies. *Journal of Climate*, 1–43. https://doi.org/10.1175/JCLI-D-21-0371.1

Yu, L., Jin, X., & Weller, R. A. (2008). *Multidecade global flux datasets from the objectively analyzed air-sea fluxes (OAFlux) project: Latent and sensible heat fluxes, ocean evaporation, and related surface meteorological variables* (p. 74). OAFlux Project Tech. Rep. OA-2008-01.

Yulaeva, E., Schneider, N., Pierce, D. W., & Barnett, T. P. (2001). Modeling of North Pacific climate variability forced by oceanic heat flux anomalies. *Journal of Climate*, *14*(20), 4027–4046. https://doi.org/10.1175/1520-0442(2001)014<4027:monpcv>2.0.co;2

Zhang, R. (2017). On the persistence and coherence of subpolar sea surface temperature and salinity anomalies associated with the Atlantic multidecadal variability. *Geophysical Research Letters*, *44*(15), 7865–7875. https://doi.org/10.1002/2017gl074342